CBN 00-6
CBX 00-22
2 June 2000
D. Cinabro
K. Korbiak

Observation of the Hourglass Effect and Measurement of CESR Beam Parameters with CLEO

Abstract

We report on the first direct observation of the hourglass effect, the waist in the luminous region of two highly focused colliding beams, at the CLEO interaction point of CESR. The observation is done with a novel technique which uses an ensemble of $e^+e^- \to \mu^+\mu^-$ events to achieve a very small resolution on the luminous region. This excellent resolution plus the large size of the CLEO II.V 4ST data set not only leads to an observation of the hourglass effect, but also enables us to measure the vertical beta star, the vertical emittance, and the bunch length.

1 Introduction

The hourglass effect[1][2] is caused by the geometry of tightly focused beams coming together at an interaction point. The beams have a "waist" at the focal point of the final quadrupoles and their size grows away from this waist. Recall that the transverse size of the beam is given by

$$\sigma(z) = \sqrt{\epsilon\beta(z)} \tag{1}$$

where $\beta(z)$ is the beta function explicitly shown to depend on the longitudinal position, z, of the beam as it travels down an accelerator and ϵ is the emittance which does not depend on z. Near a waist $\beta(z)$ can be parametrized as

$$\beta(z) = \beta^* + \frac{(z - z_0)^2}{\beta^*} \tag{2}$$

where β^* is minimum value of beta at the waist and z_0 is the position of the waist. Thus the beam in the longitudinal and transverse dimensions forms an hourglass shape with a waist at z_0.

The importance of the hourglass effect arises from the beam being in Gaussian shaped bunches with length σ_z. If the bunch length is long compared with the dimension of the waist then little of the beam is colliding where the beam is thinnest. Luminosity is not improved by making β^* smaller, with an improvement in focusing for example, if β^* is smaller than σ_z. This causes the longitudinal distribution of luminosity to depend not only on σ_z, but also on the horizontal and vertical beta stars, β^*_x and β^*_y respectively.

Table 1: CESR beam parameters at zero beam current during the 4ST running period for on 4S running.

Parameter	Value (μm)
ϵ_y	0.0084
β^*_y	17900
σ_z	18100
ϵ_x	0.21
β^*_x	1.1996×10^6

CLEO does not observe a single beam. It observes the luminous region defined by the overlap integral of the two beams. Thus we expect the longitudinal width of the luminous region to be given by

$$\sigma_{y(x)}(z) = \sqrt{\frac{\epsilon_{y(x)}}{2}\left(\beta^*_{y(x)} + \frac{(z-z_0)^2}{\beta^*_{y(x)}}\right)} \tag{3}$$

where y and x denote vertical and horizontal. The overlap integral causes the two to appear and we assume that the emittance and β^* are the same for the two beams. The beam parameters for CESR during the 4ST running period, October 1998 through February 1999, on the 4S are given in Table 1. Note that all the parameters except ϵ_y in Table 1 are given at zero beam current. The ϵ_y value is derived from the zero beam current parameters and the observed luminosity at the highest beam current. The parameters are all expected to depend on the bunch current, some in complex ways. We have observed that β^*_x [3] is reduced by roughly a factor of two at normal operating conditions. There are also observations of σ_z [4], increasing as the bunch current is increased. The ϵ_y is expected to be constant except at the very highest bunch currents, above 6 mA, where it should begin to increase.

Figure 1 shows σ_y as given by Equation 3 using the beam parameters given in Table 1. Also shown is the expected longitudinal distribution of the luminous region. This is given by[1]

$$\frac{d\mathcal{L}}{dz} = \mathcal{L}_0 \frac{\exp\left(\frac{-z^2}{\sigma_z^2}\right)}{(1+\frac{z^2}{\beta^{*2}_x})^{1/2}(1+\frac{z^2}{\beta^{*2}_y})^{1/2}} \tag{4}$$

where the expected factor of two in the denominator of the exponential disappears due to the overlap integral. The curve shown in Figure 1 takes σ_z as 19000 μm which is about what is expected in normal CLEO HEP running. Note the longitudinal distribution of the luminous region is expected to depend on β^*_y, but the β^*_x dependence is expected to be negligible. This is due to the large size of β^*_x as compared to σ_z. For the same reason we expect a negligible hourglass effect in the horizontal size of the luminous region as a function of longitudinal position.

It is easy to see from Figure 1 that in order to observe the hourglass effect at CESR with CLEO that we will need to have a resolution on the vertical size of the luminous region of order 10 μm and have a large amount of data to get a statistically useful sample at large longitudinal positions to get measures of large luminous region sizes to compare with small ones at small

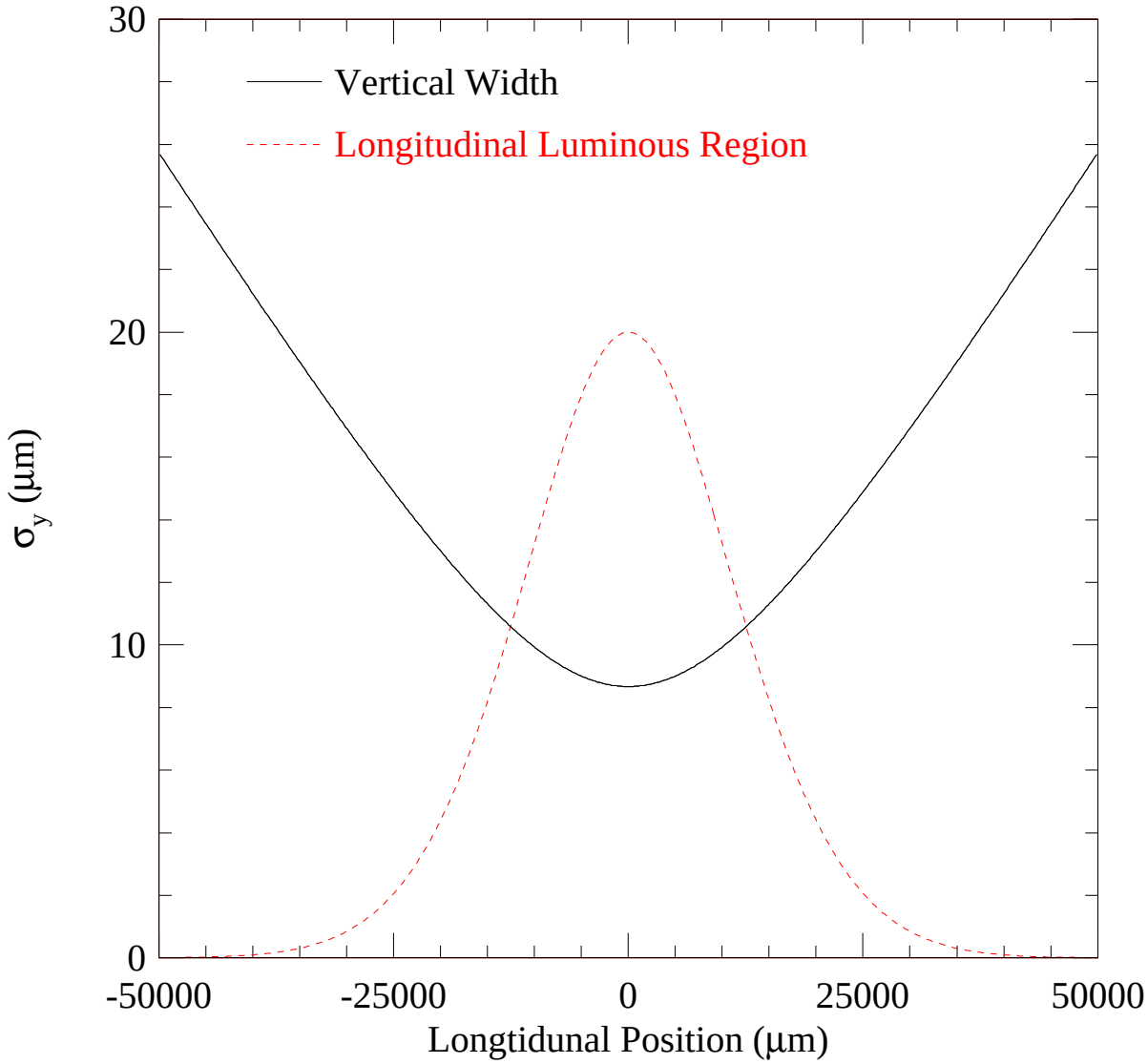

Figure 1: Expected vertical width of the luminous region as a function of longitudinal position. Also shown, in arbitrary units, is the expected longitudinal distribution of the luminous region.

longitudinal positions. Fortunately CLEO II.V has a large data set and the good resolution of the SVX that allows us to realize both of these.

Only the on 4S running of the 4ST data set is used to make this measurement. We limit ourselves to this data mainly because CESR maintained stable beam parameters throughout the running period. The on 4S data has an integrated luminosity of 1.6/fb and the off data, which is used as as a cross check and is expected to have roughly the same beam parameters, is 0.4/fb.

The next section describes the technique we use to measure the size and distribution of the luminous region. Section 3 describes the data and fitting techniques we use to observe the hourglass effect and extract the CESR beam parameters. The final section draws some conclusions.

2 The Box Technique

We begin with $e^+e^- \to \mu^+\mu^-$ events as they give the best resolution on the luminous region. These events are chosen using `KLASGL = 6`[5], `NTRKCD = 2`, both tracks must have more than 20 CD hits, at least two SVX hits in the $r\phi$ and rz views, and not be a DREDGE or Z-ESCAPE. The tracks must have opposite charge. Finally tracks used for the measurement of the luminous region must have at least three SVX hits in one of the two views.

Figure 2 shows how the box technique is implemented. The location of the center of the luminous region and its size are taken from run average data using hadronic events [3]. A box in three dimensions is centered on the measured center of the luminous region and its sides are made to be ten times the measured widths of the luminous region from the hadronic events. Tracks that pass through this box are useful for measuring the luminous region. The average position of the track inside the box is found. From an ensemble of such tracks the size and shape of the luminous region is measured.

Only tracks that pass through the box at a large angle, as shown in Figure 2, to one of the axes are useful for measurement on that axis, otherwise we simply get a measure of the center of the box. We select such tracks by cutting on the direction cosines. The placement of these cuts is essentially dictated by the size of the luminous region, which is roughly 10 μm vertically, 300 μm horizontally, and 10000 μm longitudinally. Thus a tight cut of $|\cos\theta_y| < 0.1$ is needed to measure the vertical luminous region, a looser cut of $|\cos\theta_x| < 0.3$ for horizontal, and $|\cos\theta_z| < 0.7$ for longitudinal. The same cut on $|\cos\theta_z|$ of 0.7 is also used on tracks used to make vertical and horizontal measures as the resolution degrades for tracks with large $|\cos\theta_z|$. A single track can measure at most two dimensions due to the cuts on direction cosines.

This method is tested in simulated events. We used over 100,000 $e^+e^- \to \mu^+\mu^-$ events run through the full cleog simulation and reconstructed with pass2. The predicted resolutions on the vertical, horizontal, and longitudinal beam spots are shown in Figures 3, 4, and 5 respectively. A key component of being able to measure a change in the vertical size of the luminous region is to have the vertical resolution be constant as the parameters of the tracks vary. Table 2 shows the selections we made in the simulated data to test the stability of the resolution. Key is that the vertical resolution does not depend on the longitudinal position. The only significant dependences are on tracks with large values of $|\cos\theta_z|$, which are not used due to the direction cosine cut discussed above, and on the $|\cos\theta_y|$ of the tracks. The resolution

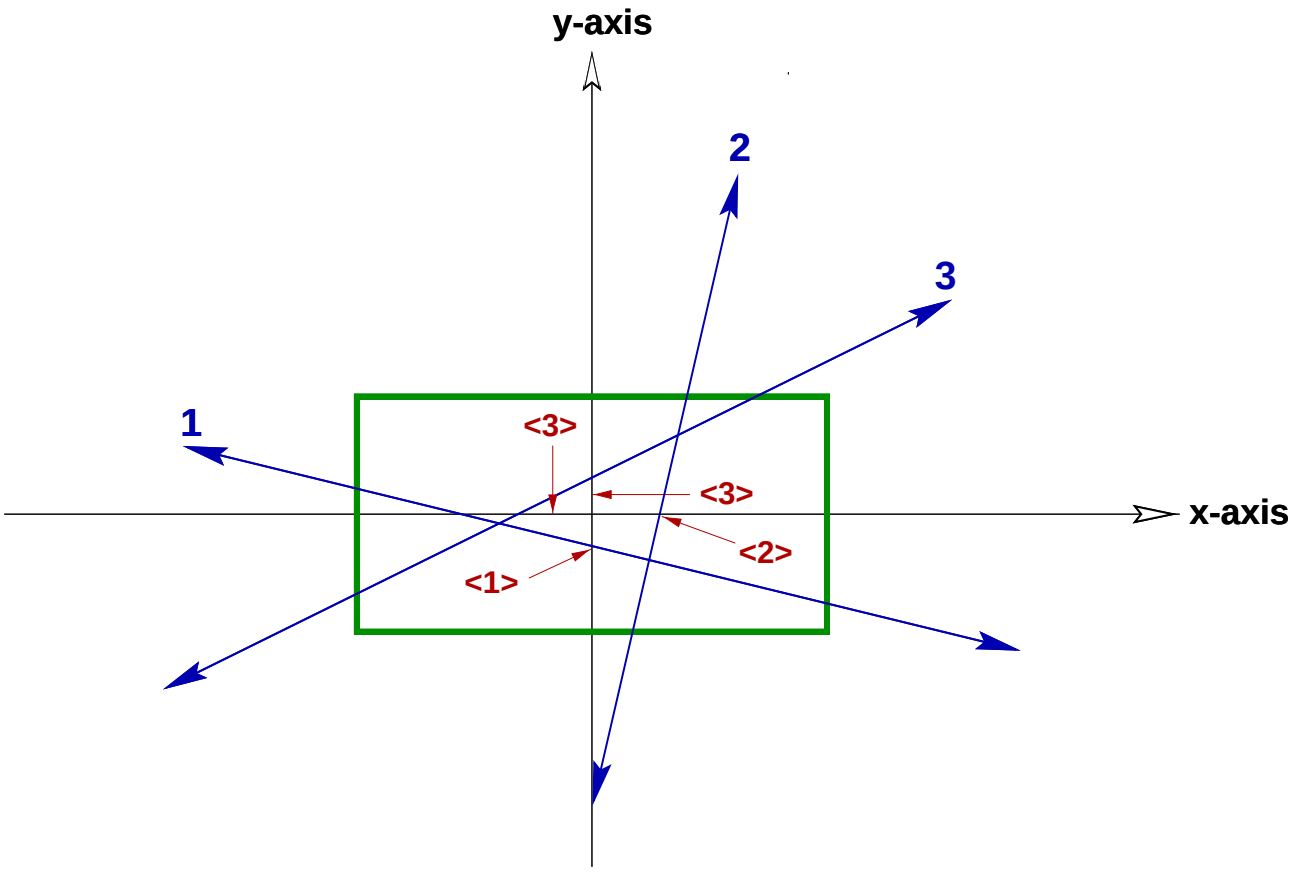

Figure 2: An ensemble of stiff tracks passing through the box allow for a precision measurement of the beam spot. For example the track labeled 1 only gives a useful measure of the vertical position of the luminous region as indicated. Track 1 crosses the the entire horizontal extent of the box and its average horizontal position is simply the center of the box. Similarly track 2 only measures the horizontal position, while track 3 measures both the horizontal and vertical positions.

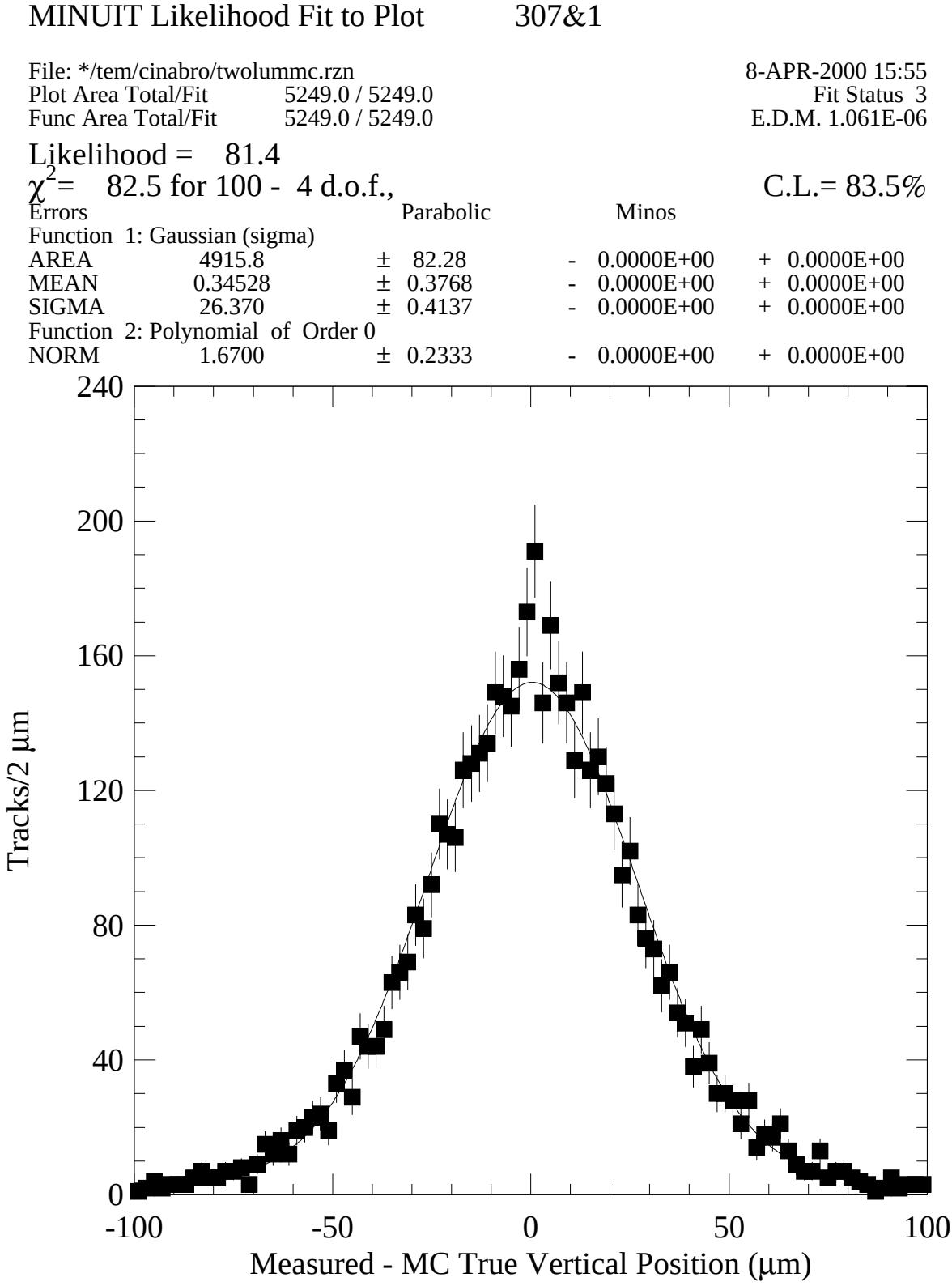

Figure 3: The resolution of the Box Technique on the vertical position of the luminous region from the simulation.

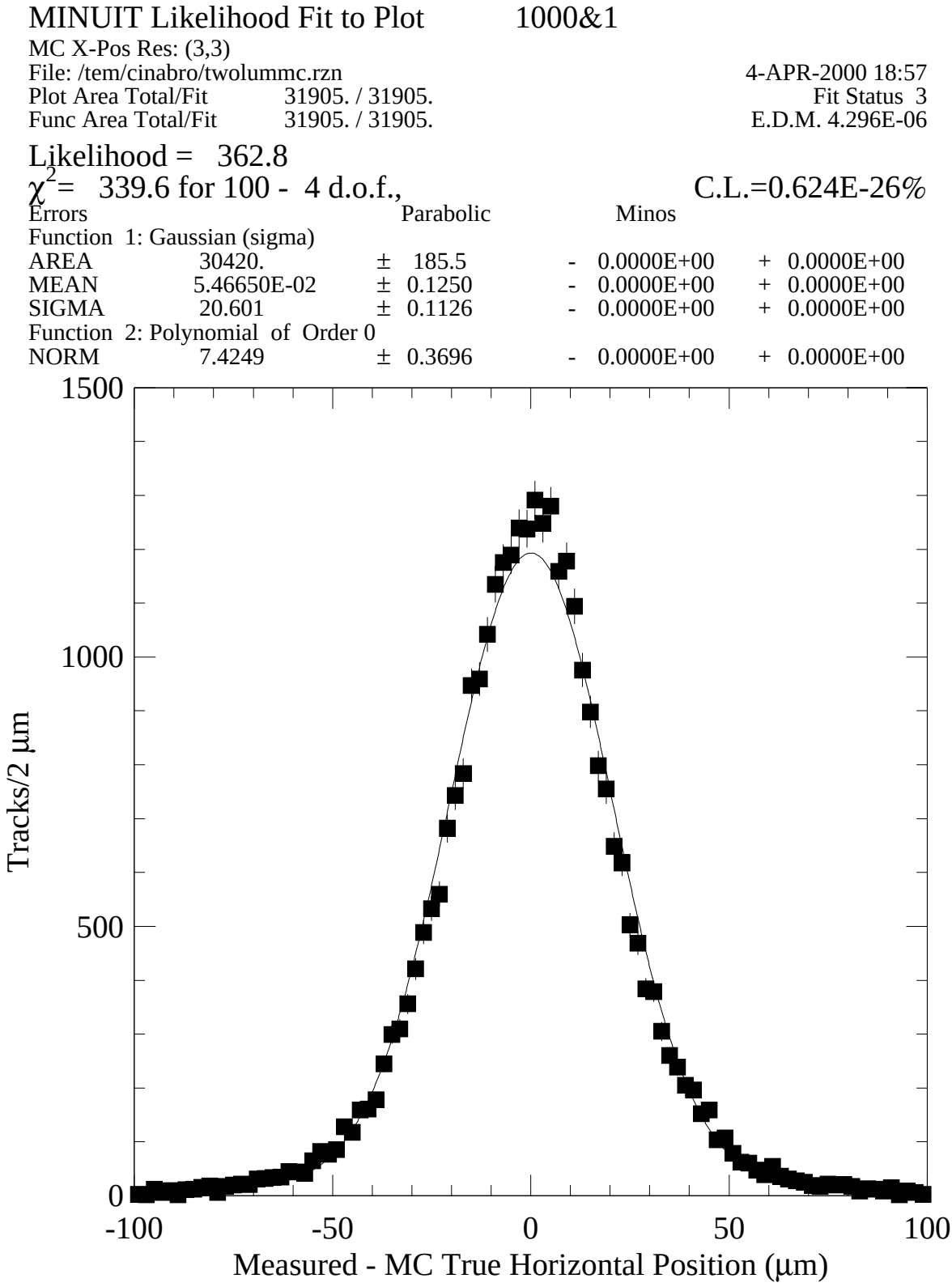

Figure 4: The resolution of the Box Technique on the horizontal position of the luminous region from the simulation.

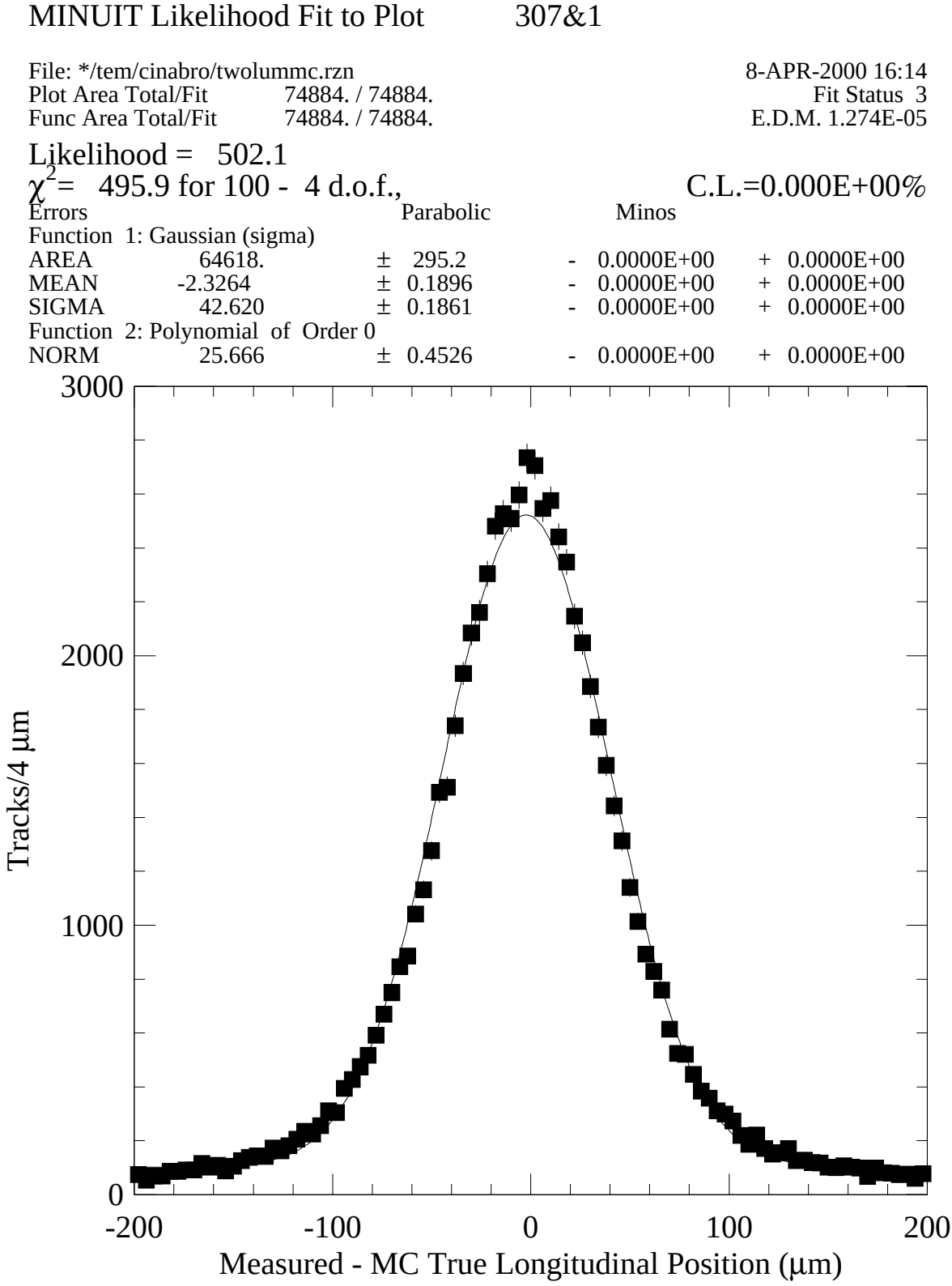

Figure 5: The resolution of the Box Technique on the longitudinal position of the luminous region from the simulation.

Table 2: Variations in the vertical resolution of the box technique as the parameters of tracks used in the box technique are changed.

Variation	Resolution (μm)
Nominal	26.37 ± 0.42
$\lvert\cos\theta_z\rvert < 0.35$	24.80 ± 0.59
$0.35 < \lvert\cos\theta_z\rvert < 0.70$	27.38 ± 0.57
$0.70 < \lvert\cos\theta_z\rvert$	32.81 ± 0.45
$\lvert\cos\theta_y\rvert < 0.09$	25.84 ± 0.40
$\lvert\cos\theta_y\rvert < 0.11$	27.21 ± 0.45
SVX Hits 2 $r\phi$, 3 z	24.40 ± 2.80
SVX Hits 3 $r\phi$, 2 z	26.18 ± 0.52
SVX Hits 3 $r\phi$, 3 z	26.74 ± 0.68
$\lvert z\rvert < 10000$ μm	26.09 ± 0.53
10000 μm $< \lvert z\rvert <$ 20000 μm	27.10 ± 0.72
20000 μm $< \lvert z\rvert$	25.00 ± 1.60

does sharply depend on the $|\cos\theta_y|$ cut. Our nominal choice of 0.1 is a compromise between a smaller cut value with improved resolution, and a larger value with decreased statistics. We include a 1.5 μm error on the resolution due to this sharp dependence.

We expect our resolution on the vertical luminous region to be yres $= 26.4 \pm 0.4 \pm 1.5$ μm with the first error to be from the statistics of our simulation sample and the second from the dependence on the $|\cos\theta_y|$ cut. Crucially we do not observe any dependence on the longitudinal position. As discussed in the next section we do not depend on the simulations prediction for the resolution as we can extract the resolution from the data itself.

The horizontal and longitudinal resolution on the luminous region, 21 and 43 μm respectively in the simulation, are much smaller than the expected sizes, and any dependences on track parameters are negligible. We ignore the horizontal and longitudinal resolutions.

3 Extraction of Beam Parameters

Using the box technique described in the previous section we look at the vertical distribution of the luminous region as a function of the longitudinal position. Figure 6 shows the vertical distribution for a small longitudinal position, and Figure 7 shows the vertical distribution for a large longitudinal position. Such distributions are fit to a Gaussian plus a flat function to account for non-beam related backgrounds as shown in the Figures. Figure 8 shows the results of these fits giving the vertical width of the Gaussians versus the longitudinal position. The hourglass effect is clearly visible.

As a cross check this procedure is repeated for the horizontal distributions and the results are shown in Figure 9. No hourglass effect is visible. The horizontal size of the luminous region is 296.1 ± 3.5 μm from fitting Figure 9 to a flat function. A fit to a second order polynomial does not produce significant linear or quadratic terms. This corresponds to a β_x^*

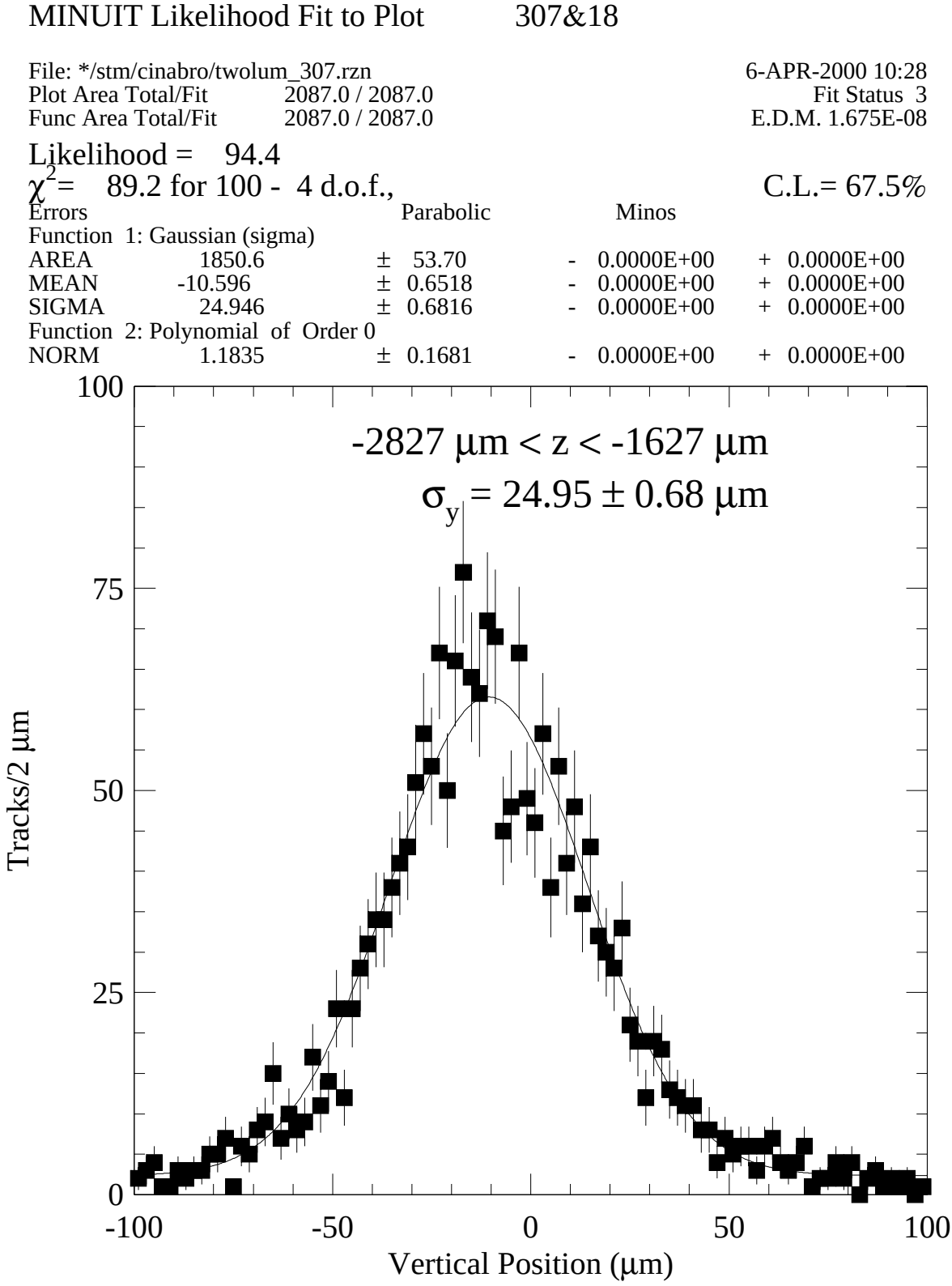

Figure 6: The vertical distribution of the luminous region for the indicated range of longitudinal positions. This is a range near the center of the longitudinal distribution.

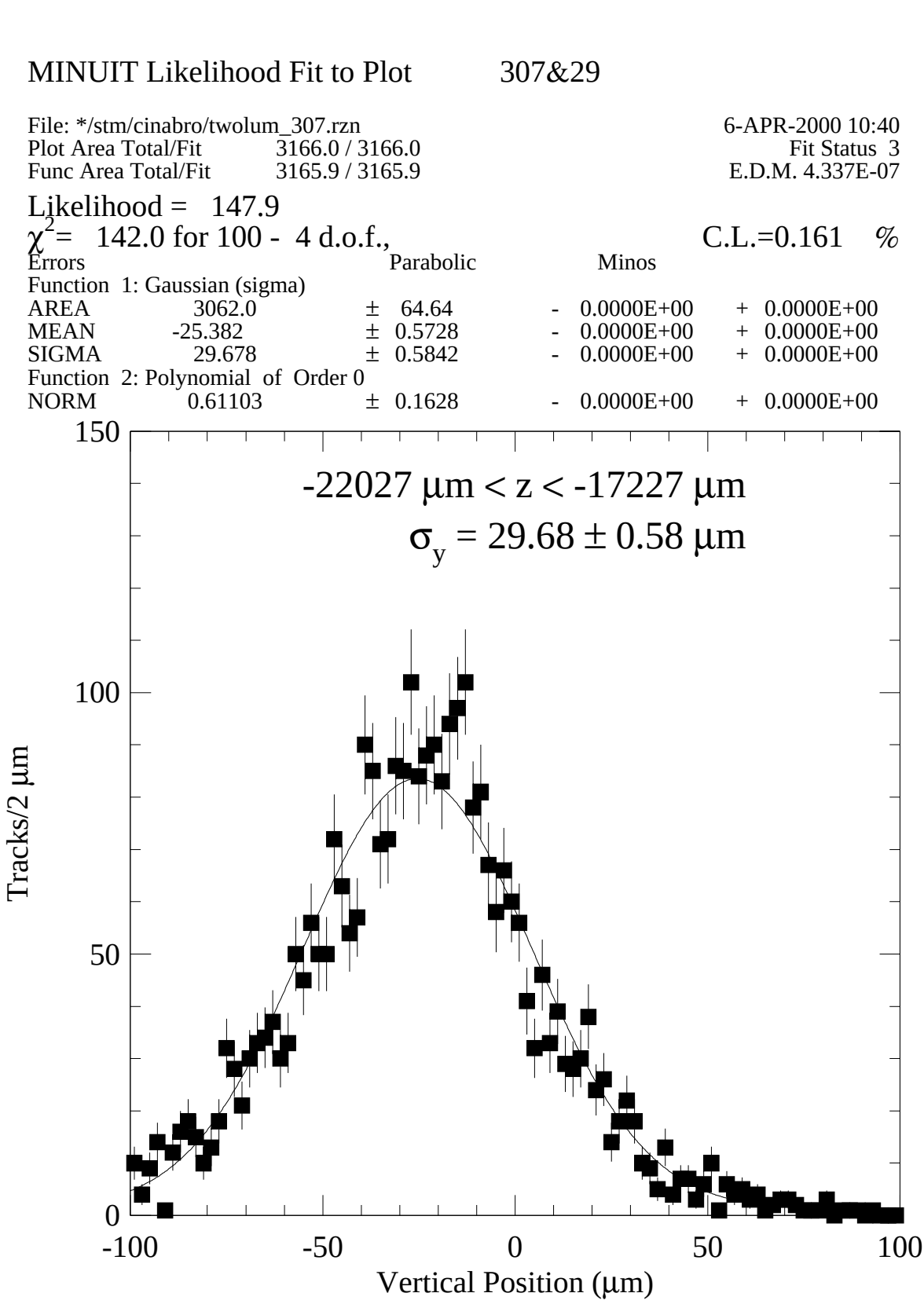

Figure 7: The vertical distribution of the luminous region for the indicated range of longitudinal positions. This is a range near the edge of the longitudinal distribution.

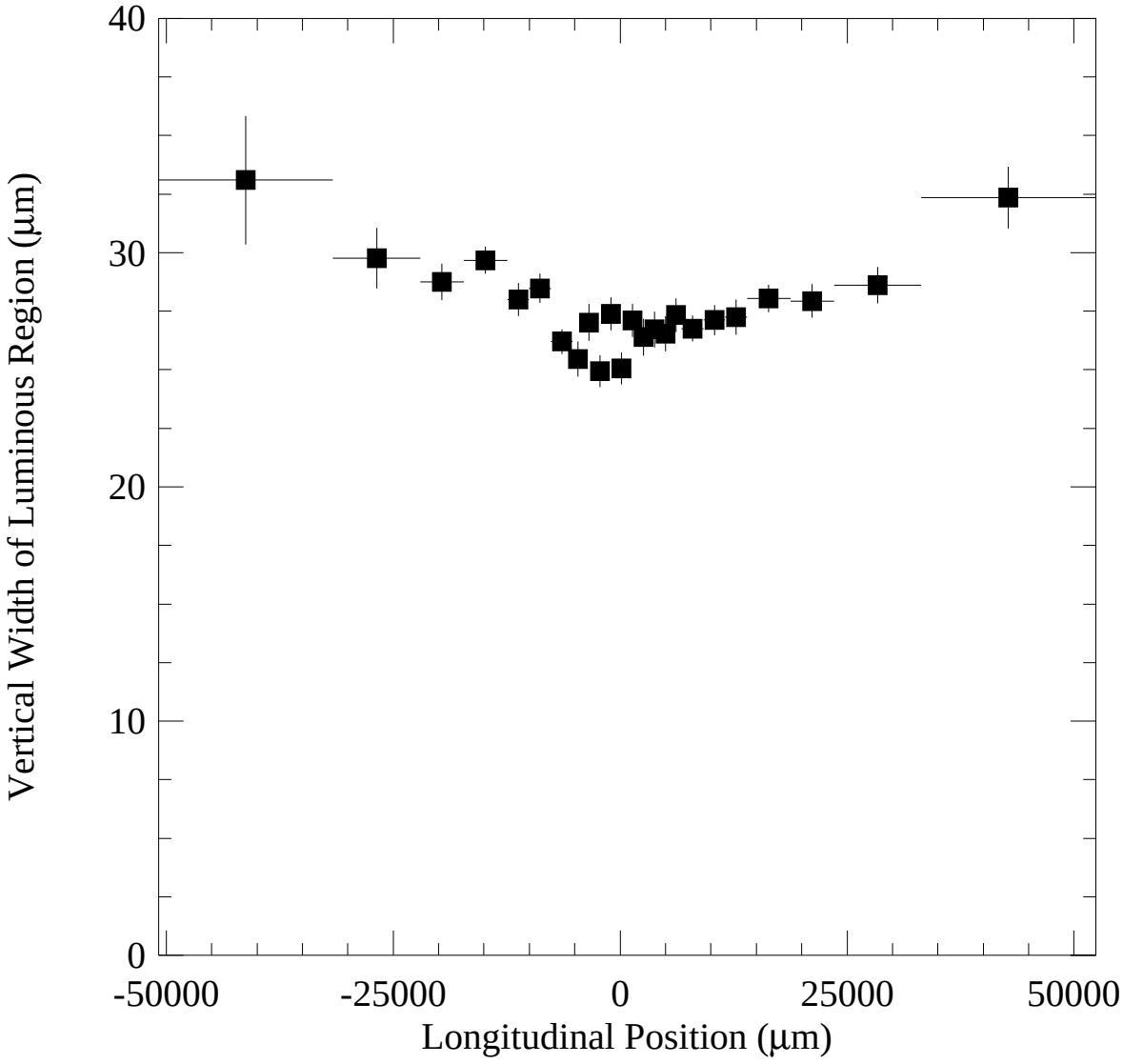

Figure 8: The vertical width of the luminous region versus the longitudinal position.

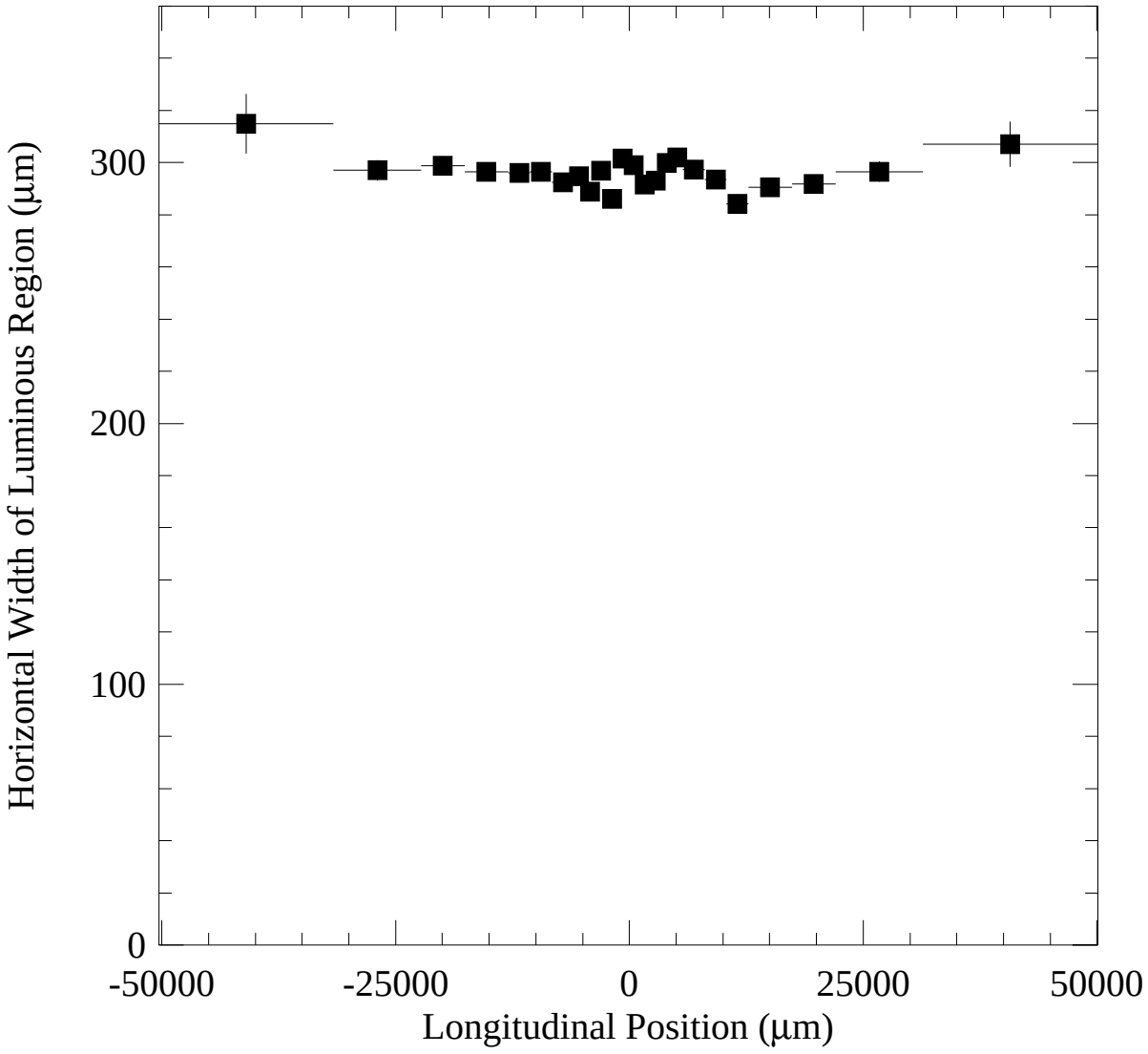

Figure 9: The horizontal width of the luminous region versus the longitudinal position.

of 417500 $\pm$ 9900 μm using the horizontal emittance, ϵ_x given in Table 1, which is in good agreement with the expectation discussed in the Introduction taking into account dynamic beta effects. Unfortunately the horizontal size of the luminous region is large and the only conclusion we can draw about the expected $\sim$ 25 μm resolution of the box technique in the $r-\phi$-plane is that it does not have a gross dependence on the longitudinal position.

We also looked at the vertical and horizontal widths versus the longitudinal positions in the 4ST off 4S data. They are in rough agreement, truthfully the vertical would agree with a flat distribution also, with the on-4S data, but with far less statistical power.

To extract the beam parameters from Figure 8 we fit the distribution to

$$\sigma_y(z) = \sqrt{\left[\frac{\epsilon_y}{2}\left(\beta_y^* + \frac{(z-z_0)^2}{\beta_y^*}\right)\right] + \mathrm{yres}^2} \tag{5}$$

where yres is the box technique's resolution on the vertical luminous region. Unfortunately such a fit does not give a useful measurement of any of the beam parameters, and not surprisingly has nearly 100% correlations among β_y^*, ϵ_y, and the resolution. We have to add more information to make such measurements.

The longitudinal distribution of the luminous region shown in Figure 10 depends on β_y^*, recall Equation 4, and can be used to provide extra information on the beam parameters and break the correlation discussed above. Unfortunately this opens up an entirely new range of questions about the box technique that need to be addressed.

Figure 5 shows the resolution of the box technique on the longitudinal position of the event production point. The resolution is about 40 μm and is negligible in comparison with the over one centimeter longitudinal size of the luminous region. In fact the box technique can be used to make a very high precision measurement of the bunch length, σ_z. This leads to a new question. As discussed in Reference [4] the bunch length depends on the bunch current and the bunches are asymmetric with their heads being narrower than their tails. It is difficult to apply the observations of Reference [4] to the measurement made here. Reference [4] was done with a different set of RF cavities and different bunch structure than this work. The functional form of the longitudinal distribution including an asymmetry in the bunch length is

$$\frac{d\mathcal{L}}{dz} = \mathcal{L}_0 \frac{\exp\left(\frac{-(z-z_0)^2}{(\sigma_z(1-\mathrm{sign}(\frac{A}{\sqrt{2}},z-z_0)))^2}\right)}{(1+\frac{(z-z_0)^2}{\beta_x^{*2}})^{1/2}(1+\frac{(z-z_0)^2}{\beta_y^{*2}})^{1/2}} \tag{6}$$

where A is the asymmetry and sign is the Fortran sign function. What we can expect a bunch length asymmetry of the order of $A = -7\%$ of the bunch size, huge on the scale of our resolution. Note that the observed size of this asymmetry is reduced by $\sqrt{2}$ in the overlap of the two bunches that produces the luminous region, but we use the single bunch length asymmetry as a parameter as defined in [4]. Figure 11 shows the bunch current distribution for the data used to measure the longitudinal distribution shown in Figure 10. This distribution has an average of 5.0 mA and an RMS of 0.8 mA. From reference [4] we expect roughly a 2% variation in the bunch length due to the bunch current distribution. This corresponds to a 4000 μm variation in the longitudinal size of the luminous region, which is huge on the scale of our 40 μm resolution. We are planning to investigate these effects further in future work.

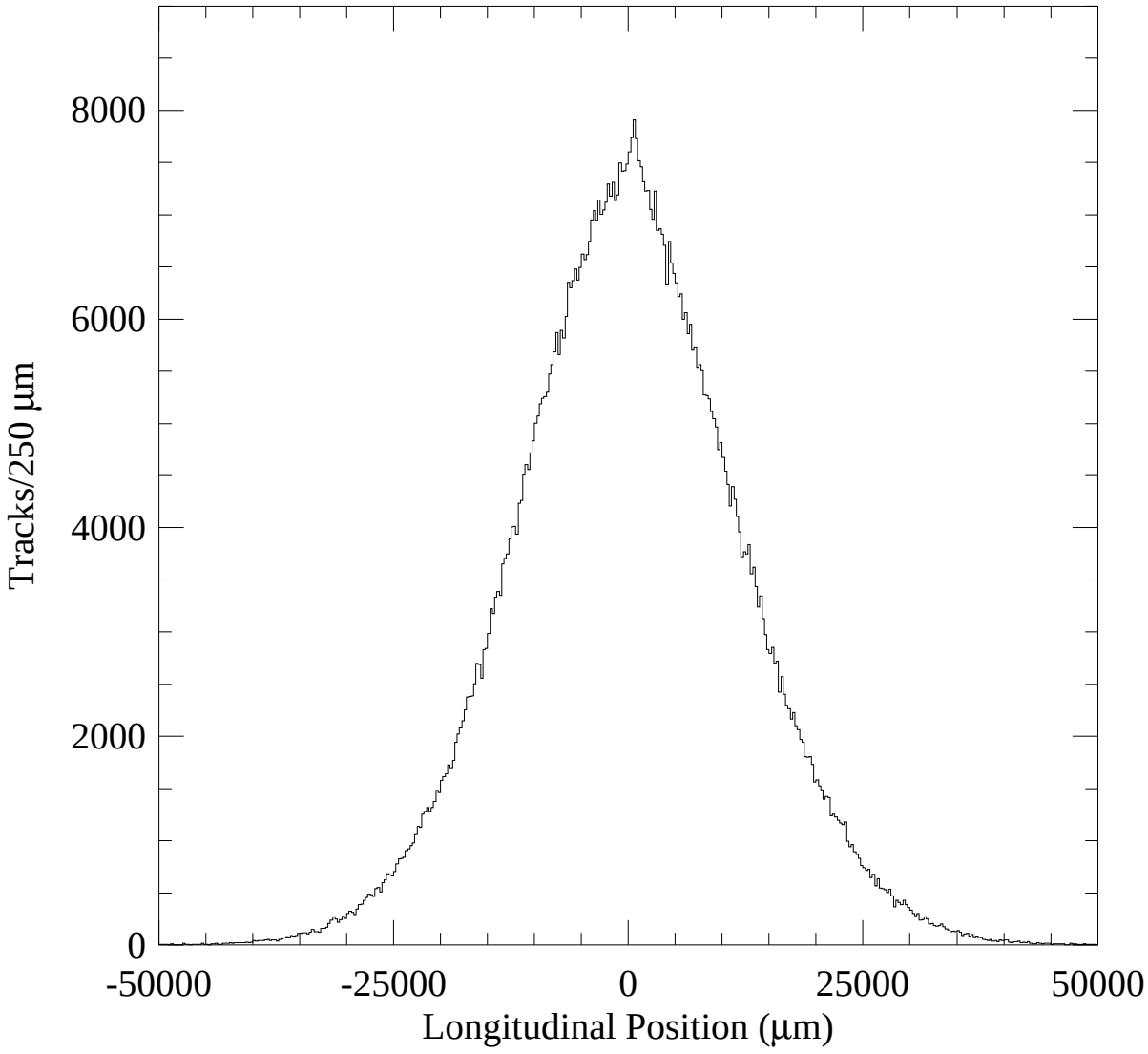

Figure 10: The raw longitudinal distribution of the luminous region.

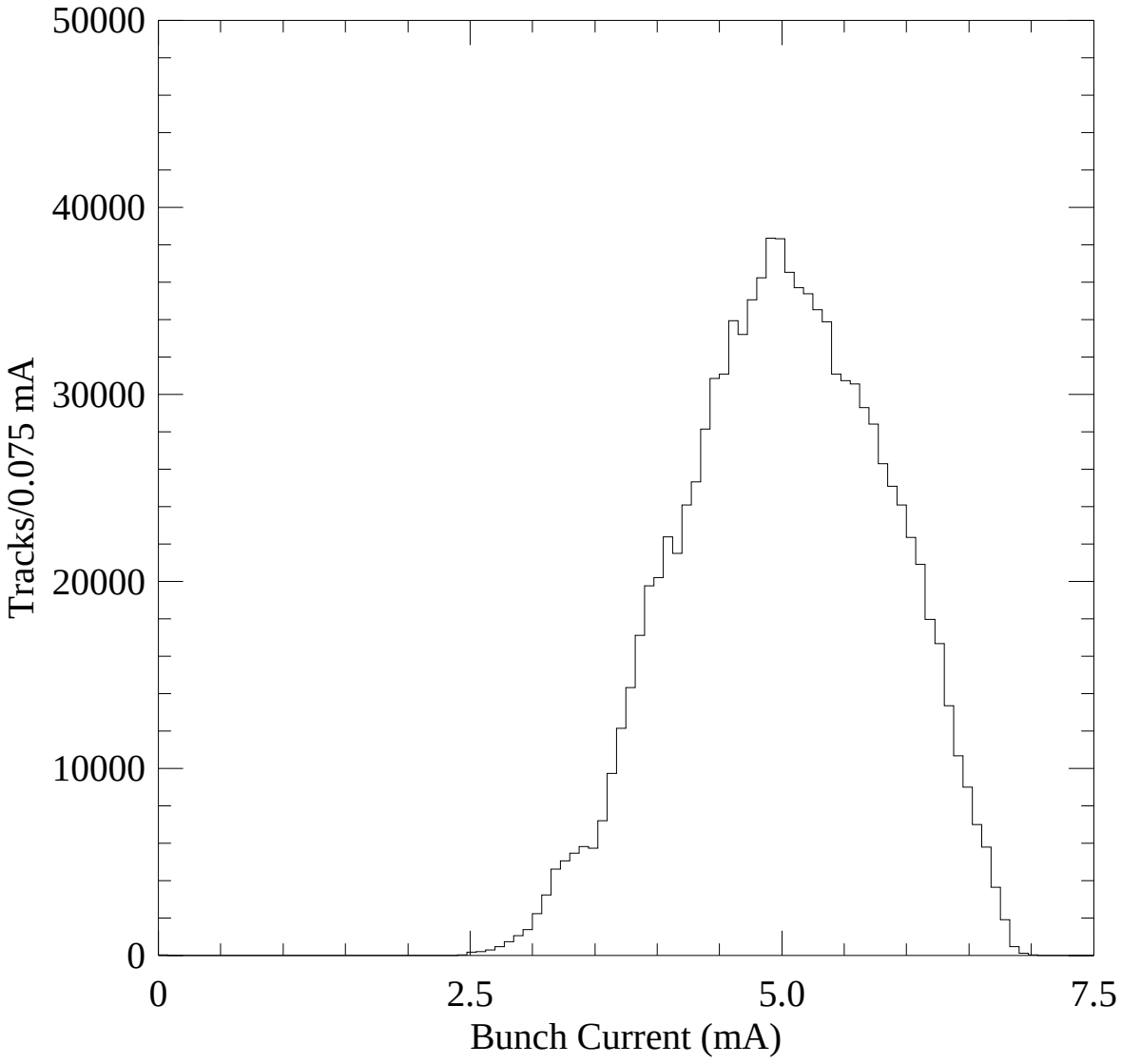

Figure 11: The average bunch current for the tracks used in measuring the luminous region.

Another confounding effect is the efficiency of the box technique on measuring the longitudinal distribution of the luminous region as a function of longitudinal position. We realized this when we tried to fit Figure 10 to the expected longitudinal shape of Equation 4 and found that the data had a sharp peak rather than the expected rounded shape. Such a fit is shown in Figure 12. Without correcting for efficiency we were unable to extract β_y^* from such fits as we found large systematic effects as we varied excluded regions to avoid the central region where it is clear that the raw data and the expectation did not agree.

Figure 13 shows the origin of this efficiency. Recall from Section 2 that we require three hits in the SVX in either the $r\phi$ or rz views of the tracks. The SVX has a dead region at its center where the ladders from the east and west ends are simply butted against each other. The gap between the two halves of the detector has been measured in surveys to be about 200 μm. In addition the edge of the silicon wafers in the detector has a non-sensitive region that extends about 400 μm from the edge of the wafer. Thus there is a ~ 1000 μm gap in the center of the detector. This gap exists for all three layers of the detector and is measured to be ~ 1000 μm to the east, negative z. Thus as shown by Figure 13 when a track points at this gap the chance for it to pass our selection criteria is reduced. Also visible is a shadow of this gap. This is caused by our selection criteria of good $\mu^+\mu^-$ events which requires two high momentum tracks, that tend to be back to back, with two hits per view in the SVX. This looser requirement is much less sensitive to the gap, but still cuts some events with one track pointing in the gap and another opposite.

These efficiency effects, which are purely geometrical, are accurately modeled by our simulation. Figure 14 is the same as Figure 13 except that it comes from simulated $\mu^+\mu^-$ events. We use the simulation to extract an efficiency for measuring the longitudinal distribution of the luminous region as a function of longitudinal position. This efficiency is shown in Figure 15. Note that at the edges of the distribution where statistics are sparse many bins are grouped together to extract an efficiency without an overwhelming statistical error. Figure 16 shows the peak region of a fit to this distribution and should be compared with Figure 12. The extraction of β_y^* in a fit to the efficiency corrected distribution is not sensitive to exclusions of the central region.

Note that such efficiency effects are small on the widths of the vertical and horizontal distributions as we are using small bins in longitudinal position and there is little variation in the efficiency for measuring the horizontal and vertical luminous region across one longitudinal position bins. We went through the exercise of applying such efficiencies derived from the simulation on the vertical luminous region data and it had a negligible effect on the fitted widths. We do not use such efficiency corrections on the vertical and horizontal widths.

The idea is to measure the beam parameters, β_y^*, ϵ_y, σ_z, and the resolution from the data in a simultaneous binned likelihood fit to the vertical width versus longitudinal position, Figure 8, and the longitudinal distribution, Figure 10 corrected by the efficiency of Figure 15. The first distribution depends on ϵ_y and the resolution, the second on σ_z and an asymmetry factor A as defined in Reference [4], and they both depend on β_y^*. The functional forms to which the data are fit are given in Equations 5 and 6. We also include a flat function in the longitudinal distribution to account for non-beam related background.

To test this simultaneous fit procedure we did toy Monte Carlo studies. The toy MC data are generated using the beam parameters given in Table 1 except for σ_z. Since we expect a range of bunch lengths to appear in our data we simulate a range of bunch lengths in the toy

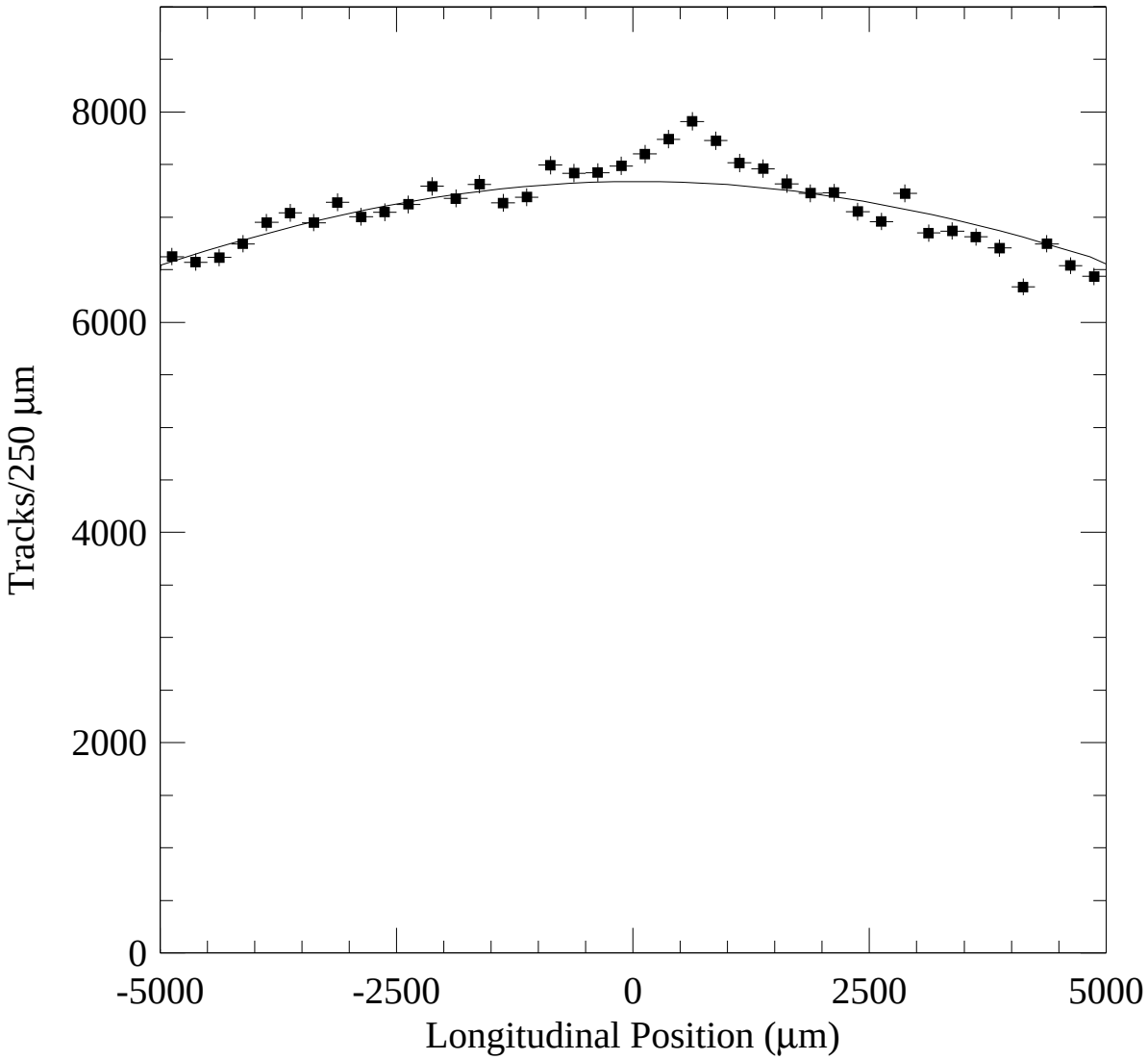

Figure 12: The central region of the raw longitudinal distribution of the luminous region. The squares are the data and the line is a fit to Equation 4.

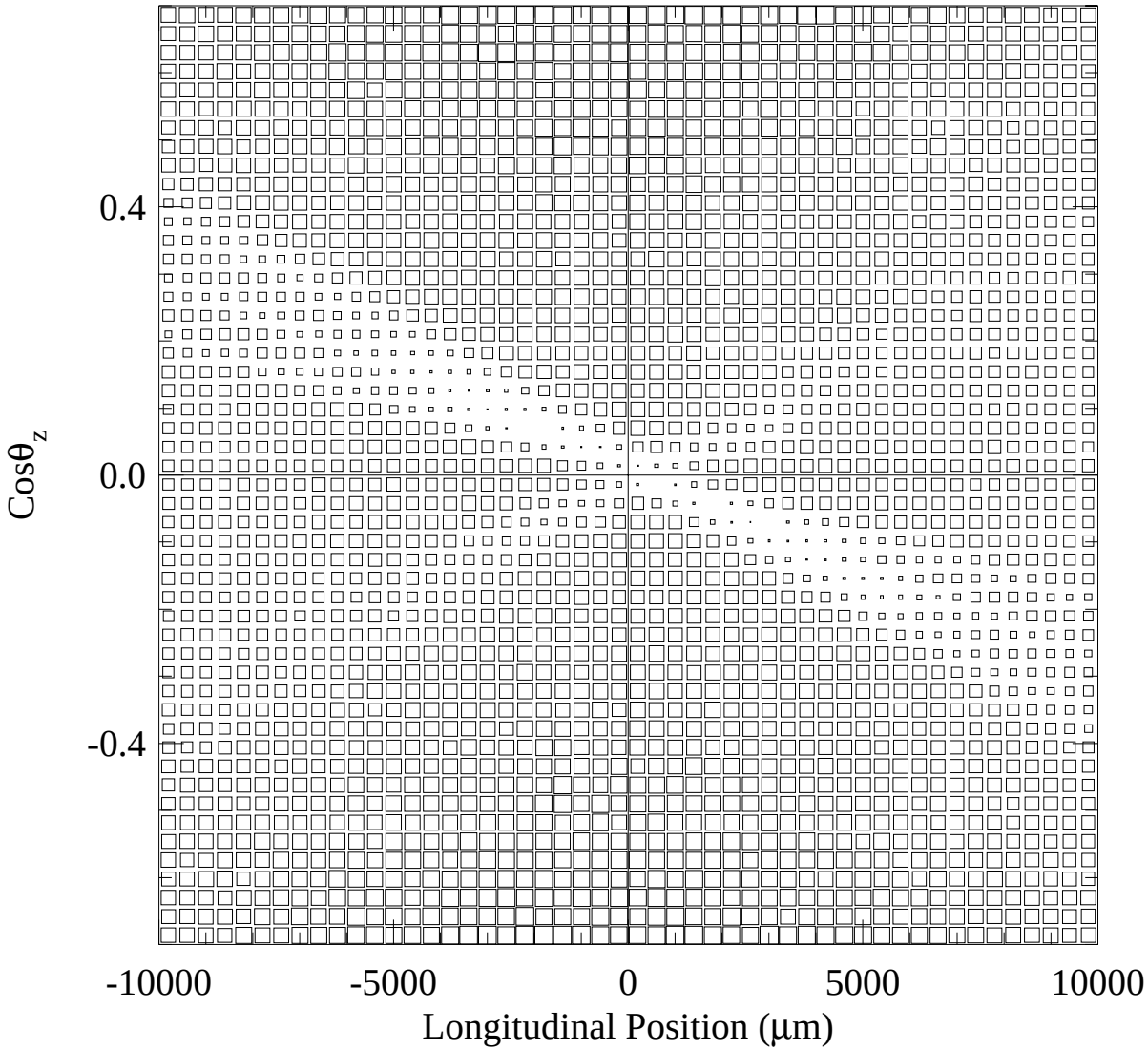

Figure 13: The z direction cosine versus the longitudinal position for tracks selected by the box technique to measure the longitudinal distribution of the luminous region. See the text for the origin of the depleted region.

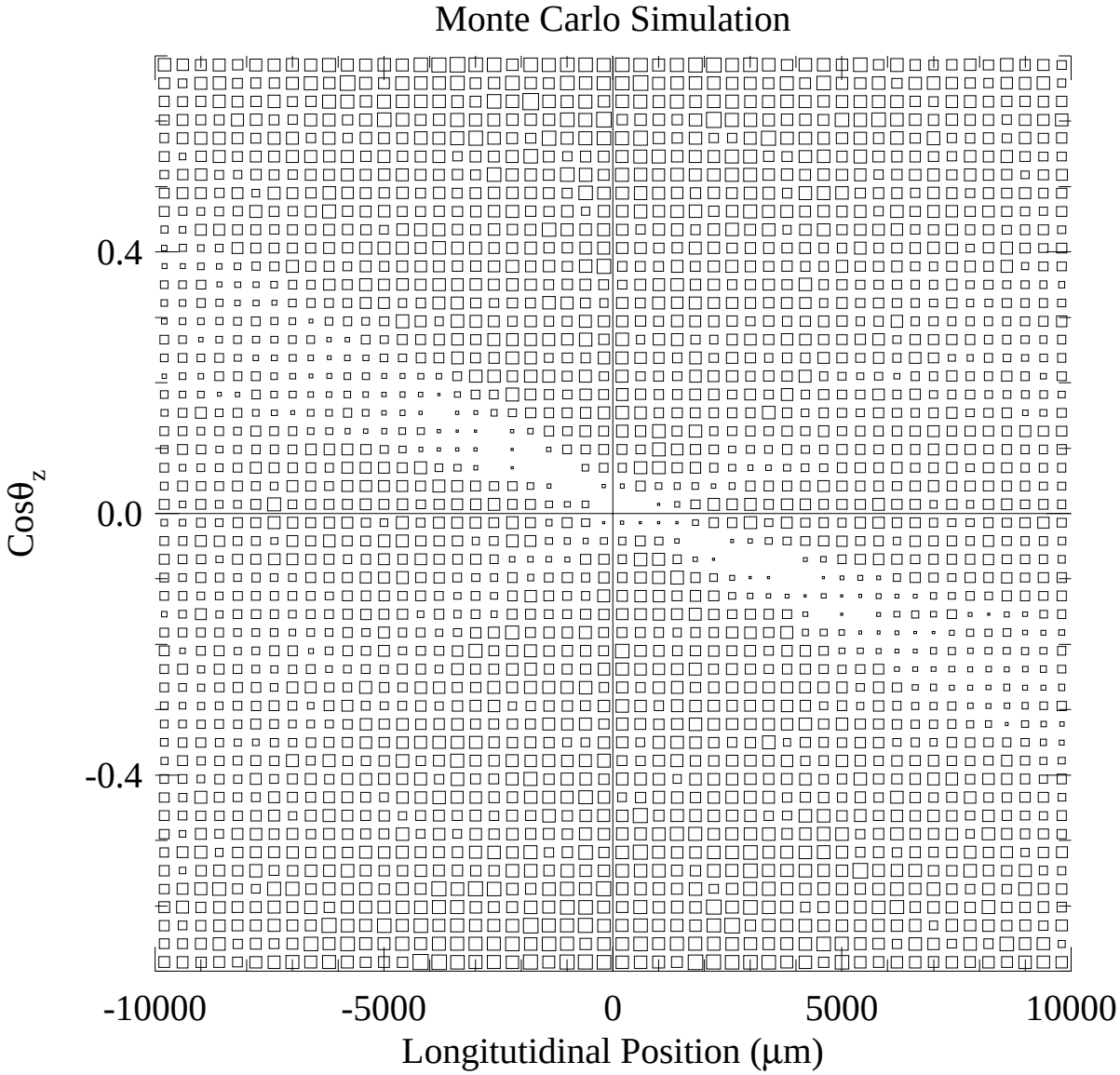

Figure 14: The z direction cosine versus the longitudinal position for tracks selected by the box technique to measure the longitudinal distribution of the luminous region in the simulation. Compare with Figure 13.

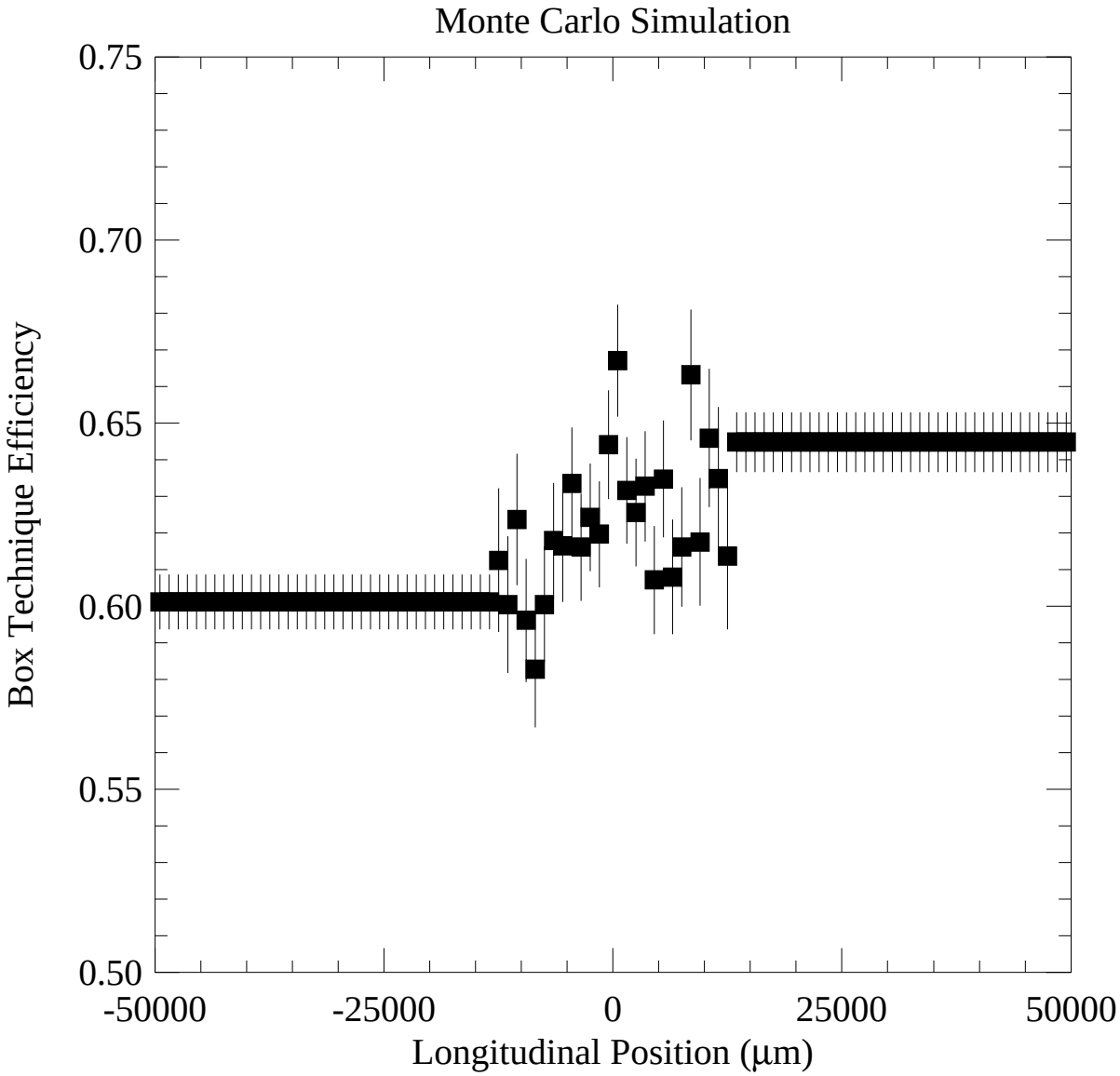

Figure 15: The efficiency from the simulation for the box technique to select tracks to measure the longitudinal distribution.

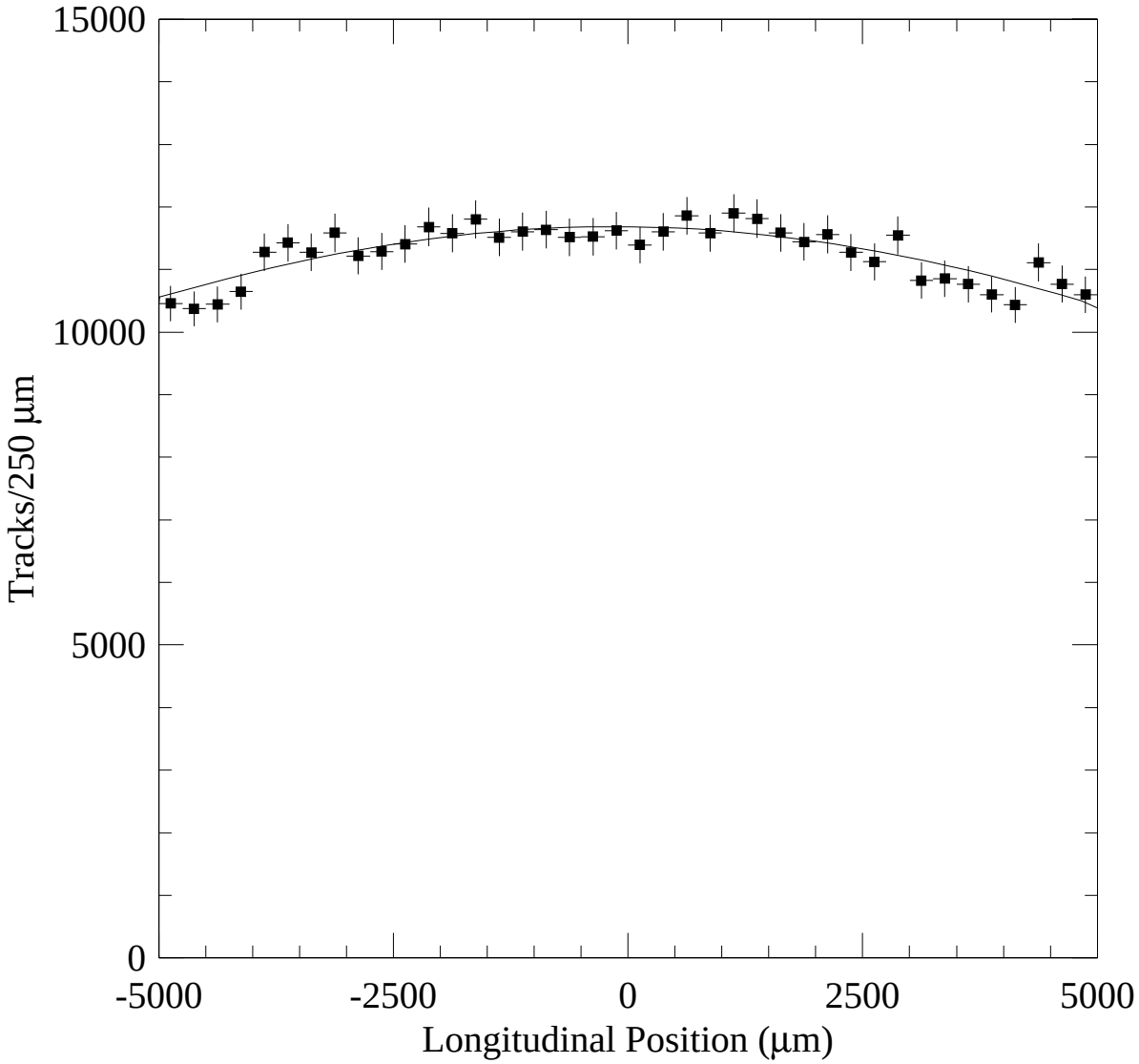

Figure 16: The central region of the efficiency corrected longitudinal distribution of the luminous region. Compare with Figure 12.

Table 3: The range of bunch lengths simulated in our Toy Monte Carlo data.

Fraction of Toy MC Data (%)	σ_z (μm)
1.0	18700
3.0	18800
7.6	18900
16	19000
23	19100
19	19200
18	19300
10	19400
1.8	19500
0.6	19600
Average	19151

Table 4: Results from fits to 100 toy MC distributions as described in the text.

Parameter	Input (μm)	Fitted Value (μm)	Pull Mean	Pull Width
β_y^*	17900	17910 ± 170	0.00 ± 0.12	1.229 ± 0.087
ϵ_y	0.0084	0.0097 ± 0.0029	0.39 ± 0.20	1.89 ± 0.14
σ_z	See Table 3	19152 ± 37	0.02 ± 0.13	1.311 ± 0.093
resolution	26	25.8 ± 1.7	-0.01 ± 0.12	1.163 ± 0.082

MC data. That range is based on the range of bunch currents we are observing in Figure 11 and the observations of Reference [4] and is given in Table 3. The toy MC used a resolution of 26 μm to smear the underlying vertical width distribution. The toy MC also models statistics appropriate for our observed data.

An example of a fit to toy MC data is shown in Figure 17. One hundred such distributions were generated and fit. The results of this toy MC study are shown in Table 4. Notable features are that the simultaneous fit procedure seems to work very well. All but one of the pull distributions are consistent with normal distributions. The exception is ϵ_y which gives a pull distribution with a width of 1.89 ± 0.14. This seems to indicate that the error on ϵ_y expected from the toy MC study and given in Table 4 is a factor of two too small. This is caused by some of the toy data fits which gave a value for ϵ_y close to zero with unrealistically small errors. Fortunately the fit to the data does exhibit this behavior. Also the toy MC studies showed that the correlations among β_y^*, ϵ_y, and the resolution were still large, but not 100%. The toy MC also tells us that we expect a likelihood of 676 ± 55 from our fit.

Another thing we learned from the toy MC is that this fit is not sensitive to β_x^*. For both the toy MC study and the data fit we fix $\beta_x^* = 417500$ μm based on our observation in Figure 9 and discussed above. The results of the fits to both the toy MC and real data change negligibly when β_x^* is allowed to float. The resulting values for β_x^* from such fits are consistent with 417500 μm but with large errors of $\sim 5 \times 10^5$ μm.

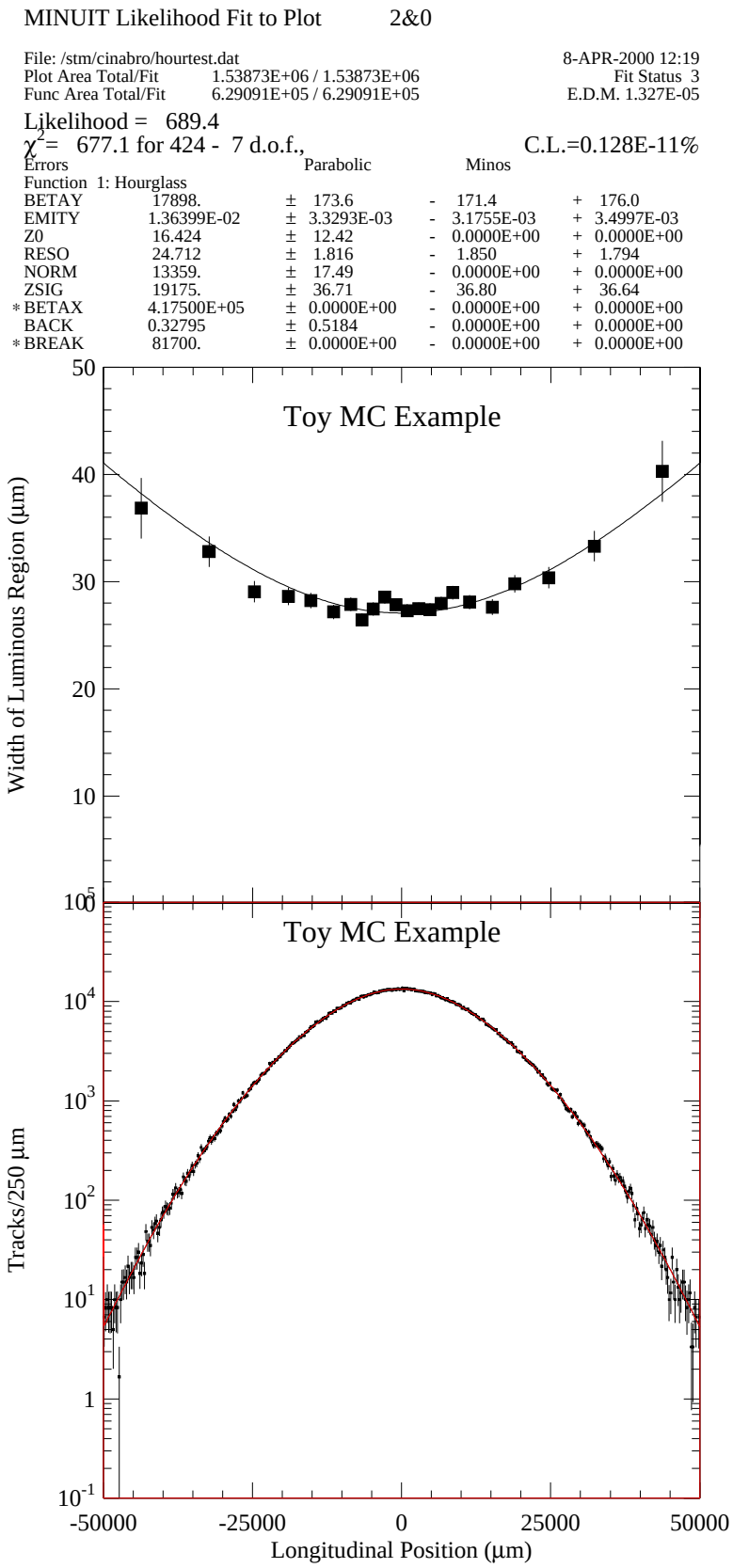

Figure 17: An example fit to toy MC data as described in the text.

Table 5: The results of the simultaneous fit to the data distributions for the vertical width of the luminous region as function of longitudinal position and the longitudinal distribution.

Parameter	Fitted Value (μm)
β_y^*	17330 ± 170
ϵ_y	$0.0070 + 0.0054 - 0.0047$
σ_z	19052 ± 38
resolution	25.5 ± 1.9
z_0	-1076 ± 34
Asym	$(-6.18 \pm 0.23)\%$

Table 6: The correlation coefficients for the fit of Figure 18 and Table 5.

	Correlation Coefficient					
Parameter	β_y^*	ϵ_y	σ_z	yres	z_0	A
β_y^*	1.000	0.015	-0.907	-0.014	0.160	0.120
ϵ_y		1.000	-0.013	-0.796	0.003	0.002
σ_z			1.000	0.013	-0.140	-0.103
yres				1.000	0.000	0.000
z_0					1.000	0.919
A						1.000

Figure 18 and Table 5 shows the results of our fit to the data. The results are in good agreement with both our error expectations from the toy MC study from Table 4, and the expected CESR beam parameters of Table 1 and Reference [4]. Note that we get very accurate measures of β_y^* and σ_z, a resolution from the data consistent with our expectation of 26.4 ± 1.6 μm from the simulation, but only a 1.5 standard deviation measure of ϵ_y. The error on ϵ_y is what we would have predicted from the toy MC study discussed above. We do get a likelihood much larger than than expected from the toy MC study, 1592.8 versus the 676 ± 55. All of this increase in likelihood comes from large absolute values of longitudinal positions in the longitudinal distribution. This is most likely due to our unrealistic modeling of the various bunch lengths in the data as a discrete set of bunch lengths in the toy MC. When we went from one bunch length to many bunch lengths in the toy MC the likelihood increased by a factor of two.

Shown in Table 6 are the correlation coefficients among the important parameters of the fit. These also agree with our expectations from the toy MC. In summary it appears that our fit to the data is actually measuring the average bunch length and the vertical beta star. There are comparatively large systematic effects discussed below.

In a final attempt to improve our measure of ϵ_y we repeat the data fit described above with the resolution fixed to 26.4 μm as predicted by the simulation. This fit does give a slightly improved measurement of ϵ_y of 0.0053 ± 0.0030 μm with the other parameters changing negligibly. When the fixed resolution is varied by ± 1.5 μm as indicated by our simulation

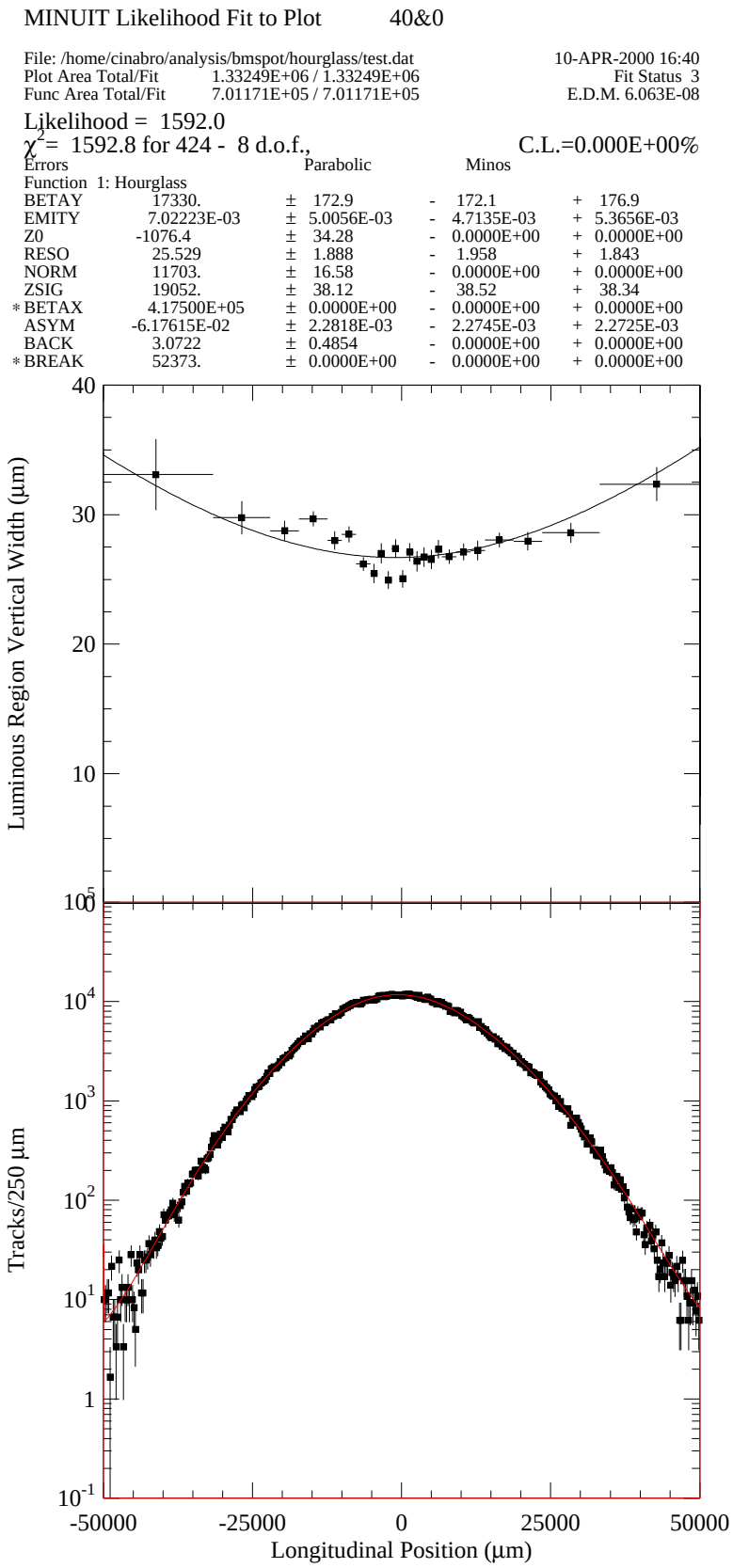

Figure 18: The simultaneous fit to the data distributions for the vertical width of the luminous region as function of longitudinal position and the longitudinal distribution.

Table 7: Summary of systematic effects. All values are in μm.

Source	β_y^*	ϵ_y	σ_z
Fit Procedure	± 198	± 0.0010	± 94
$\lvert\cos\theta_y\rvert$ cut variation	± 0	± 0.0012	± 0
$\lvert\cos\theta_z\rvert$ cut variation	± 240	± 0.0005	± 150
Track Selection	± 220	± 0.0010	± 75
Efficiency and MC Stats	± 250	± 0.0002	± 60
Quadrature Sum	± 456	± 0.0019	± 201

studies described above this introduces an error of ± 0.0021 μm on ϵ_y. The combined error of ± 0.0037 μm on $\epsilon_y = 0.0053$ μm is consistent with and not a substantial improvement over the results of Table 5. We prefer to quote results for the fit where the resolution is left floating.

We varied our standard fit to test its robustness. We excluded the positive and negative z data from the fit, we excluded the data at small longitudinal positions and at large longitudinal positions, and we used a χ^2 fit rather than a likelihood fit. The only parameters that showed significant disagreement with the standard result were β_y^* and σ_z. We include systematic errors of ± 198 μm on β_y^* and ± 94 μm on σ_z due to the fit procedure.

We varied other facets of the analysis and repeated the procedure described above to estimate systematic effects. We varied the cuts on the direction cosines, ± 0.01 on $\cos\theta_y$ and ± 0.1 on $\cos\theta_z$, we relaxed the three SVX hits in one view to the more standard two hit per view requirement, we varied our procedure for applying the efficiency as a function of the longitudinal position to one that used constant bin sizes, and we used the simulation efficiency without errors as an estimate of the effects of our limited simulation statistics. For all these variations the change in the central values of the beam parameters from the standard procedure is taken as the systematic effect The systematic errors we have estimated from these variations are summarized in Table 7.

While checking for systematic effects we made plots of the other parameters of the Gaussian fits to the vertical and horizontal luminous region distributions besides the widths. Figure 19 shows the mean of the vertical distributions as a function of the longitudinal position. This shows that the luminous region has an offset of -10 μm and a slope of 65 μm/10 cm at the interaction point. No such effect is visible in the horizontal distributions where the same distribution is flat with a scatter of about 10 μm. This slope is consistent with the method that is used to determine the zeros for the longitudinal, vertical, and horizontal distributions described in Reference [3]. That method has a resolution on the width of the luminous region of ~ 100 μm and an error on the mean of ~ 10 μm. The normalization of the Gaussian fits versus the longitudinal position is shown in Figure 20. This strange shape caused us a great deal of consternation when we first observed it, but we realized that it is caused by the cuts on the direction cosines in y and z and the box technique which has a very narrow y extent. This shape is reproduced in the simulation, and we even wrote a toy Monte Carlo simulation that only included the direction cosine cuts and the box technique and reproduced the strange shape. The horizontal normalizations versus longitudinal position produces a similar, but less extreme, shape that is also properly modeled by the simulation and the toy MC. Neither of

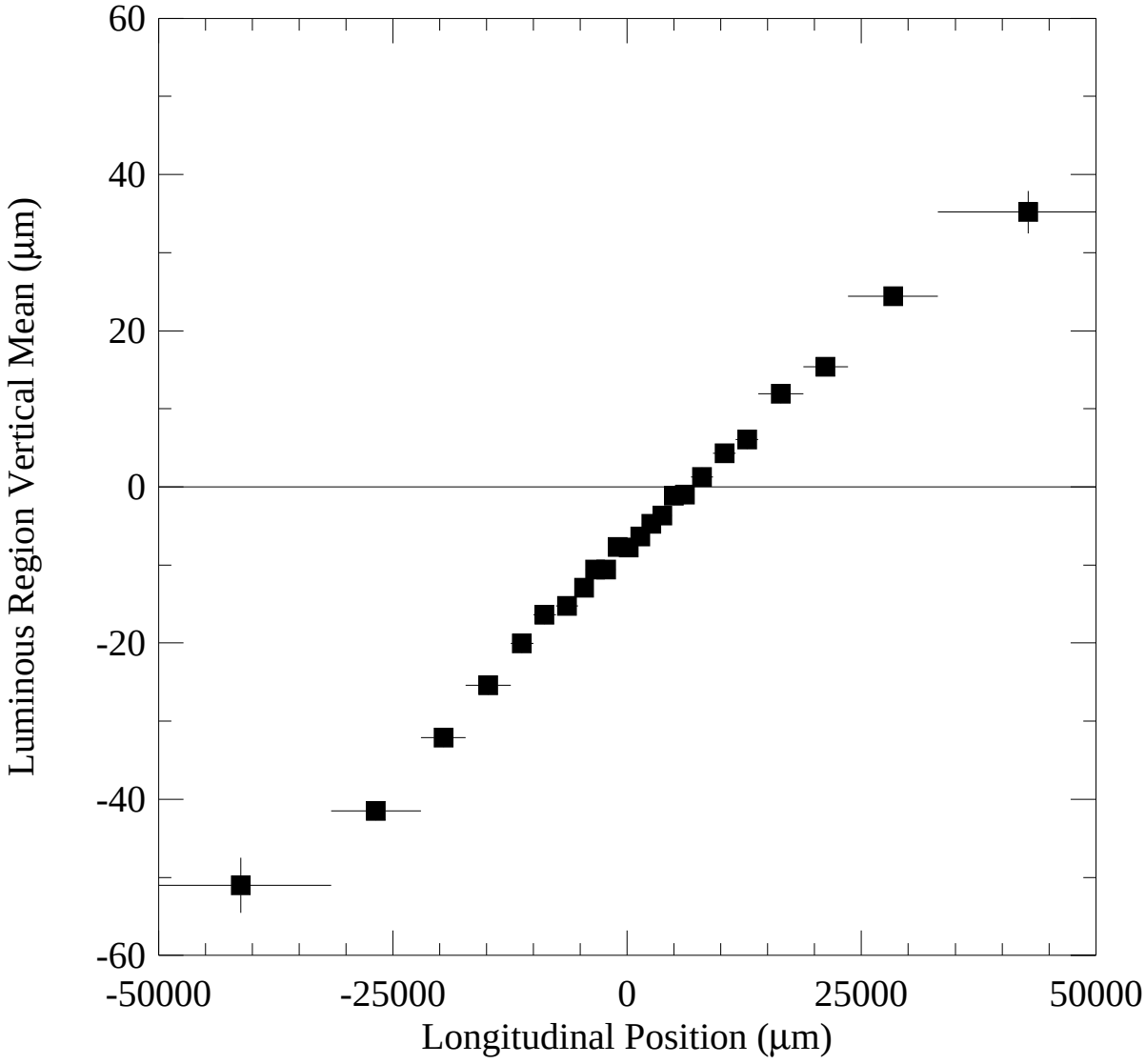

Figure 19: The vertical mean of the luminous region as function of the longitudinal position.

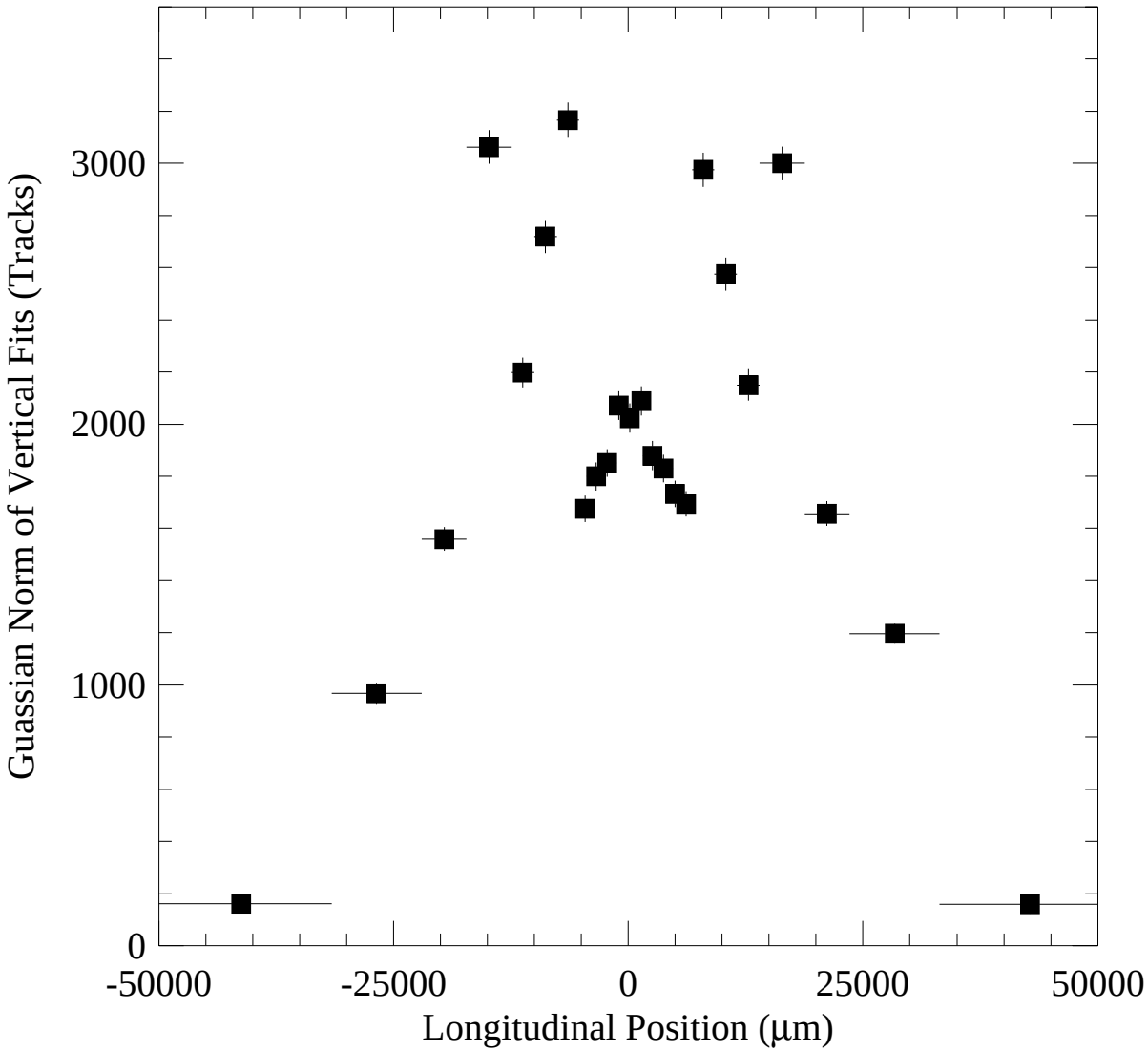

Figure 20: The normalization of the Gaussian fits of the luminous region as function of the longitudinal position.

these effects has any impact on the extraction of the beam parameters. They are included here for completeness and as a warning to other CLEO analyses which might be sensitive to them.

4 Conclusion

We have used a new method, called the box technique which takes advantage of the hit resolution in the CLEO II.V SVX in $e^+e^- \to \mu^+\mu^-$ events, to measure the size of the luminous region of CESR at the CLEO interaction region. The technique has a resolution of 25.5 ± 2.0, which is extracted from a fit to the data and agrees well with the prediction of our simulation. The excellent resolution of the box technique combined with the large size of the CLEO II.V data set allows us to directly observe the hourglass effect, the increase in the size of the luminous region away from the focal point, for the first time. We are also able to extract the CESR beam parameters

$$\beta_y^* = (17330 \pm 170 \pm 460)\ \mu\text{m}, \quad (7)$$

$$\epsilon_y = (0.0070 \pm 0.0054 \pm 0.0019)\ \mu\text{m}, \quad (8)$$

$$\sigma_z = (19050 \pm 40 \pm 200)\ \mu\text{m}, \quad (9)$$

where the first error is statistical and the second is systematic, by simultaneously fitting the vertical width of the luminous region as a function of the longitudinal position and the distribution of the longitudinal luminous region. This is the first direct observation of the hourglass effect. With a substantial degradation in the resolution $e^+e^- \to e^+e^-$ events can be used, and the box technique, can be used as a real time monitor of the size and shape of the luminous region.

References

[1] CBN 89-1, S. Milton.

[2] M. A. Furman, PAC 91, p. 422.

[3] CBX 96-94/CBN 96-17 and CBX 97-39/CBN 97-14, D. Cinabro.

[4] CBN 99-9 and CBN 99-10, R. Holtzapple, *et al* and R. Holtzapple, *et al*, Phys. Rev. ST Accel. Beams **3**, 034401.

[5] CSN 96-347, A. Weinstein.